Analysis of the Effect of Enhanced FOV and Sampling Strategy on the Spatial Resolution Enhancement of Spaceborne Microwave Radiometer

Zhou Zhang, Zhenzhan Wang, Wenming He, and Xiaolin Tong

***Abstract*—Higher spatial resolution can improve the application ability of spaceborne microwave radiometer data. To investigate the capability to enhance the spatial resolution of the radiometer measurements, we analyzed the effect of enhanced field of view (FOV) and sampling strategy on improving spatial resolution using the Backus–Gilbert (BG) method, with the scanning parameters of FengYun-3D Microwave Radiation Imager (MWRI) as an example. The results suggest that selecting an appropriate enhanced FOV and increasing the sampling overlap rate can yield better spatial resolution and effectively reduce the brightness temperature (BT) error that arises from resolution enhancement. As an example, the MWRI 18.7 GHz channel with a spatial resolution of 30 × 50 km is taken. When the spatial resolution of the enhanced FOV is set to 25 × 35 km, compared with other options, the average BT error caused by resolution enhancement is reduced to 0.38 K, and the spatial resolution is improved to 27.3 × 40.5 km. In addition, when the sampling overlap rate of cross-track and along-track directions is set to 91.4% × 92.4%, the highest in the experimental conditions, compared with the original sampling setting, the average BT error caused by resolution enhancement is reduced from 0.72 to 0.4 K, and the spatial resolution is improved to 22.8 × 35.7 km. These experimental findings may provide insights into designing future radiometers and applying the BG method.**

***Index Terms*—Enhanced field of view (FOV), sampling strategy, spaceborne microwave radiometer, spatial resolution enhancement.**

I. Introduction

SPACEBORNE microwave radiometer can realize the effective monitoring of ground conditions in most cases, but its main disadvantage is low spatial resolution. Higher spatial resolution can be achieved through physical means or data processing. From a physical perspective, the spatial resolution can be improved by increasing the aperture of the antenna. However, the high cost of installing large antennas for the spaceborne microwave radiometer remains a challenge due to satellite payload size and weight limitations. Therefore, the use of data processing methods to improve spatial resolution has been extensively studied.

Data processing methods can be roughly divided into data fusion methods and methods based on antenna pattern inversion. The former ones mainly improve spatial resolution by incorporating additional information from complementary observations [1]. For example, methods combining radar and optical data with microwave radiometer data [2], [3], methods for combining measurement data acquired from high-frequency and low-frequency channels of the multichannel microwave radiometer based on the iterative image reconstruction algorithm [4] or the smoothing filter-based image modulation technique [5], and the method of using deep neural network and degradation models to learn high-frequency channel data [6], [7], [8]. On the other hand, antenna pattern inversion methods are defined as the linear inversion problem of antenna pattern deconvolution [9]. This method improves the spatial resolution of passive microwave images by linearly combining the brightness temperature (BT) observations in overlapping areas of footprints based on the antenna pattern [8]. Typical methods include the Backus–Gilbert (BG) method [10], [11], [12], the wiener filtering method [13], [14], the scatterometer image reconstruction (SIR) algorithm [15], the method based on p-norm minimization [16], [17], [18], etc. The BG method is based on the matrix inverse algorithm to reconstruct a smaller equivalent antenna pattern and improve spatial resolution. The Wiener filtering method restores the image by eliminating the low-pass filtering effect caused by the antenna pattern. The SIR algorithm reconstructs the BT through iterative gradients. The method based on p-norm minimization uses regular energy norm in Hilbert space and Banach spaces to solve the reconstruction.

While the data fusion method typically achieves better resolution enhancement, incorporating additional information may result in damage to the original information contained in the low-frequency channel data [8]. In comparison, the antenna pattern

Manuscript received 29 March 2023; revised 31 May 2023 and 16 August 2023; accepted 19 August 2023. Date of publication 23 August 2023; date of current version 14 September 2023. This work was supported by the National Key Research and Development Plan under Grant 2022YFB3903303. *(Corresponding author: Zhenzhan Wang.)*

Zhou Zhang and Wenming He are with the Key Laboratory of Microwave Remote Sensing, National Space Science Center, Chinese Academy of Sciences, Beijing 100190, China, and also with the School of Electronic, Electrical and Communication Engineering, University of Chinese Academy of Sciences, Beijing 100049, China (e-mail: zhangzhou191@mails.ucas.ac.cn; hewenming18@mails.ucas.ac.cn).

Zhenzhan Wang and Xiaolin Tong are with the Key Laboratory of Microwave Remote Sensing, National Space Science Center, Chinese Academy of Sciences, Beijing 100190, China (e-mail: wangzhenzhan@mirslab.cn; tongxiaolin@nssc.ac.cn).

Digital Object Identifier 10.1109/JSTARS.2023.3308038

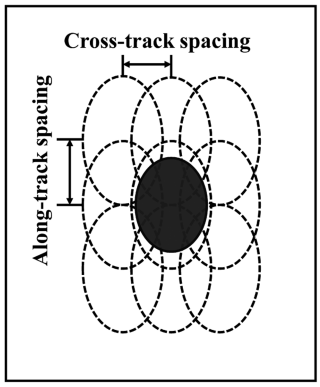

Fig. 1. Relative position distribution between the source FOVs and the enhanced FOV. The shape composed of dotted lines is the source FOV, and the shape composed of solid black lines is the enhanced FOV. The distance between adjacent source FOVs represents the sampling interval.

inversion method is more widely used and does not affect the original channel information, but may introduce additional BT errors [19]. Furthermore, the ability to improve spatial resolution is limited by the observation characteristics of the radiometer, which may not meet practical application needs. Therefore, exploring the relationship between observation characteristics and spatial resolution enhancement capabilities is crucial for the system design of the radiometer and the application of antenna pattern inversion methods.

The BG method is a commonly used spatial resolution enhancement method for the spaceborne microwave radiometer based on the antenna pattern inversion method. It has been applied to a variety of existing loads, including Special Sensor Microwave/Imager [20], Soil Moisture Active Passive [21], Advanced Microwave Scanning Radiometer-2 [22], [23], Microwave Radiation Imager (MWRI) [24], etc. The BG method calculates the weight contribution of the antenna pattern of the channel to be enhanced (source pattern) to the antenna pattern of the target channel (target pattern) in the enhanced field of view (FOV) based on the relative position relationship between the source pattern FOVs. The goal is to obtain the synthesized pattern as close as possible to the target pattern by weighting the source pattern. The relative position distribution between the source pattern FOVs (source FOVs) and the enhanced FOV, and the sampling interval between adjacent source FOVs are illustrated in Fig. 1. The solution process of the BG method indicates that the sampling strategy and the spatial resolution of the enhanced FOV are crucial factors affecting the effect of spatial resolution enhancement. However, in current studies, the observation FOV of adjacent channels with higher spatial resolution than the source channel is usually fixedly selected as the enhanced FOV, and only the sampling strategy of the instrument itself is considered. The effect of enhanced FOV and sampling strategy on spatial resolution enhancement has not been systematically analyzed.

Therefore, to investigate the capability to enhance the spatial resolution of the radiometer measurements, we take the observation geometry of FengYun-3D MWRI as an example, and use the BG method to simulate and analyze the effect of enhanced FOV resolution and sampling strategy on the spatial resolution enhancement capability. Moreover, the BT error caused by spatial resolution enhancement is also analyzed.

Our contributions in this article are summarized as follows.

1) The effect of enhanced FOV with different resolutions on spatial resolution enhancement is analyzed. The result suggests that better spatial resolution enhancement can be achieved by selecting an appropriate enhanced FOV in the BG method.
2) The effect of different sampling overlap rates on spatial resolution enhancement is analyzed. The experimental result may provide a reference for the system design of spaceborne microwave radiometer missions in the future.

The rest of this article is organized as follows. The MWRI and BG method are introduced in Section II. The simulation and evaluation parameters are introduced in Section III. The experimental results are provided in Section IV. Finally, Section V concludes the article and in Section VI discussion is given.

II. Instrument and Method

A. Microwave Radiation Imager

The MWRI has ten observation channels covering 10–89 GHz. The relevant parameters and channel information are given in Table I [25]. As depicted in Fig. 2(a), MWRI flies at an altitude of 836 km, the main reflector has a viewing angle of 45° to the ground, the incident angle on the surface is about 53.1°, and the scanning width on the earth is 1400 km. The scanning method is a fixed viewing angle conical scanning method with uniform circular motion. A total of 266 observation samples are obtained per scan rotation.

Since all channels of MWRI use the same geographic location information, such as longitude, latitude, incidence, and azimuth, the locations of sampling points on the earth surface for different channels are consistent. The difference in observation FOVs between channels is mainly reflected in different spatial resolutions, as shown in Fig. 2(b). The solid lines in different colors represent the FOVs of different channels, respectively.

B. BG Method

According to the principle of multichannel radiometer scanning imaging, the antenna BT $T_A(\rho_A)$ of a certain channel at ρ_A can be expressed as

$$T_A\ (\rho_A) = \int G\left(\rho_A, \rho\right) T_B\left(\rho\right) d\rho \tag{1}$$

where $T_B(\rho)$ is the surface BT, and $G(\rho_A, \rho)$ is the antenna pattern in a certain channel. Based on (1), the antenna BT $T_A(\rho_0)$ of a certain channel at ρ_0 can be expressed as a linear combination of a set of T_{Ai} [10]

$$T_A\ (\rho_0) = \sum_{i=1}^{N} a_i T_{Ai} \ = \int \left[\sum_{i=1}^{N} a_i G_i\left(\rho\right)\right] \ T_B\left(\rho\right) dA. \tag{2}$$

The core of the BG method is to find the optimal weight factors a_i of N adjacent observations T_{Ai}, and then reconstruct the quantity closest to the true measurement value T_A. Based on (2), the objective function can be set as an integral of the

TABLE I
MWRI INSTRUMENT CHARACTERISTICS

Channel (GHz)	Polarization	3 dB Footprint (km)		Sampling Interval (km)		Beam Width
		Cross-track	Along-track	Cross-track	Along-track	
10.65	V/H	51	85	6	11	2.01°/2.03°
18.7	V/H	30	50	6	11	1.18°/1.17°
23.8	V/H	27	45	6	11	0.99°/0.99°
36.5	V/H	18	30	6	11	0.62°/0.62°
89	V/H	9	15	6	11	0.29°/0.29°

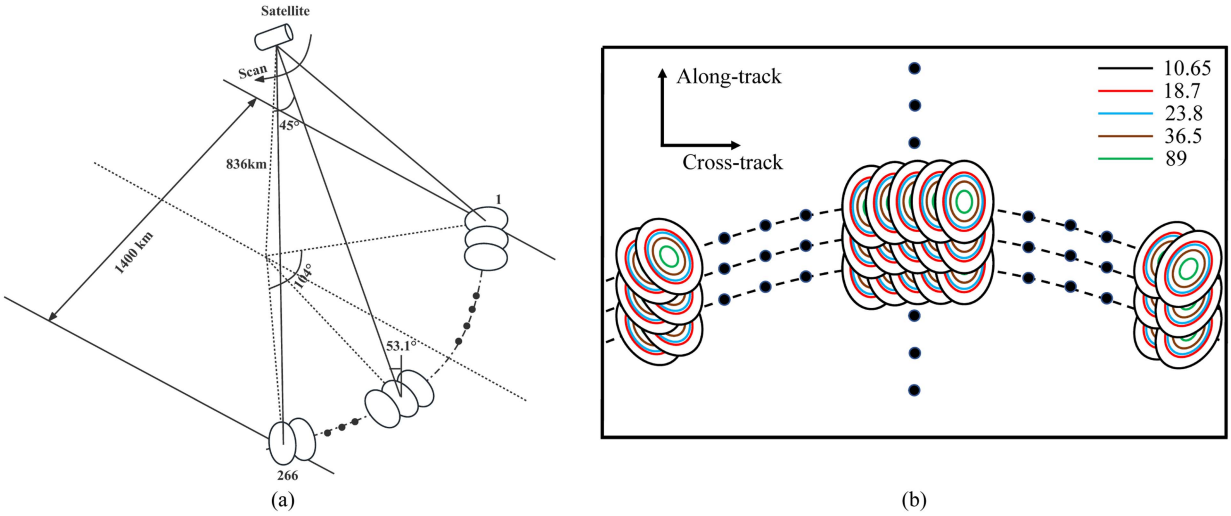

Fig. 2. Schematic of MWRI observation geometry. (a) MWRI on-orbit observations. (b) Spatial distribution of the FOVs on the earth surface in different channels of MWRI.

following form:

$$Q_0 = \int \left[\sum_{i=1}^{N} a_i G_i - F \right]^2 dA \tag{3}$$

where F is the target pattern. In addition, the data measured by the microwave radiometer are also mixed with noise signals. Based on (2), the variance of random noise in the synthetic solution of BT can be expressed as

$$e^2 = \boldsymbol{a}^T \boldsymbol{E}\boldsymbol{a} \tag{4}$$

where $\boldsymbol{E}$ is the noise covariance matrix. As the noise is purely random and hence no correlation exists between successive measurements, $\boldsymbol{E}$ is a diagonal matrix whose diagonal elements are the random noise variance in T_{Ai} [10]. To reduce the amplification level of instrument noise, the objective function Q is introduced by combining Q_0 and e^2

$$Q = Q_0 \cos\gamma + e^2 \omega \sin\gamma \tag{5}$$

where ω is the dimensional tuning parameter and γ is the tradeoff parameter. ω is used to ensure that Q_0 and e^2 are consistent in scale. γ varies from 0 to $\pi/2$ to balance noise and resolution enhancement effect. When $\gamma = 0$, only the improved spatial resolution is considered, and when $\gamma = \pi/2$, only the noise suppression is considered. Under the premise of $\int \sum_{i=1}^{N} a_i G_i dA = 1$, the weight factors obtained after minimizing Q by the Lagrange multiplier method can be expressed as

$$a = \boldsymbol{V}^{-1} \left[\boldsymbol{v} \cos\gamma + \frac{1 - \boldsymbol{u}^T \boldsymbol{V}^{-1} \boldsymbol{v} \cos\gamma}{\boldsymbol{u}^T \boldsymbol{V}^{-1} \boldsymbol{u}} \boldsymbol{u} \right] \tag{6}$$

where $\boldsymbol{V}$, G_{ij}, u_i v_i can be expressed as

$$\begin{cases} V = G\cos\gamma + \omega \boldsymbol{E} \sin\gamma \\ G_{ij} = \int G_i(\rho) G_j(\rho) dA \\ u_i = \int G_i(\rho) dA \\ v_i = \int G_i(\rho) F(\rho) dA \end{cases}. \tag{7}$$

The process for calculating weights using the BG method for a single sampling point is presented above. In the calculation process of the BG method, the value to measure the noise amplification before and after the spatial resolution enhancement is called the Noise Factor. Based on (4), it can be expressed as

$$\text{Noise Factor} = \sqrt{\boldsymbol{a}\boldsymbol{a}^{\mathbf{T}}}. \tag{8}$$

In the process of applying the BG method, it mainly involves the selection and adjustment of tradeoff parameter and adjacent points. For the selection of γ, to enhance resolution without amplifying noise, the γ is selected when the Noise Factor is less than or equal to 1 in the subsequent experiments. For the selection of adjacent points, only the candidates with v above the

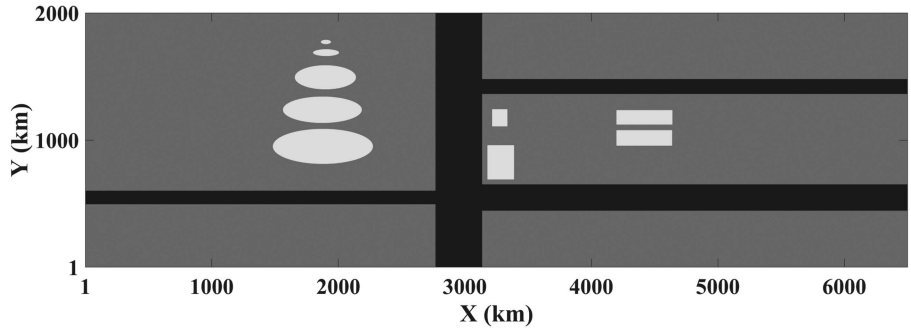

Fig. 3. BT distribution of the reference field. The gray area represents the background, with a BT value of 270 K. The white and black areas represent different ground objects, with BT values of 300 and 245 K, respectively.

cutoff level are selected, for which a_i are calculated. The cutoff level chosen in this article is -30 dB of the maximum v [22]. Moreover, more detailed information about the BG method can be found in [10].

III. Simulation and Evaluation Parameters

For the simulation experiment, we generated a simulated BT reference field to represent the BT range of the land surface. The field measures 6500 $\times$ 2000 km with a resolution of 1 pixel/km, and the BT range is between 235 and 310 K, as shown in Fig. 3. The gray area represents the background of the reference field, with a BT value of 270 K. The white and black areas represent different ground objects on the reference field, with BT values of 300 and 245 K, respectively.

To objectively analyze the quality of spatial resolution enhancement, fit error (FE) and root mean square error ($RMSE$) are introduced, as shown in the following equation:

$$FE = \int \left| F - \sum_{i=1}^{N} a_i G_i \right| \, dA \tag{9}$$

$$RMSE = \sqrt{\sum_{y=1}^{n} \sum_{x=1}^{m} \left(I_{(x,y)} - J_{(x,y)} \right)^2 / m * n}. \tag{10}$$

FE is defined as the absolute difference between the target pattern and the synthesized pattern at a sample point. In (9), F is the target pattern, a_i are the optimal weight factors calculated by the BG method, G_i are the adjacent source patterns, and $\sum_{i=1}^{N} a_i G_i$ is the synthesized pattern. Noted that previous studies have suggested that the main reason for FE is the large sidelobe effect of the synthesized pattern. A large FE can lead to abnormal BT changes in the image after resolution enhancement [23]. To provide an overall evaluation of the resolution enhancement, the average FE of all sampling points is used in the following experiments.

$RMSE$ is a measure of the difference between two images. In (10), $I_{(x,y)}$ and $J_{(x,y)}$ are the pixel values of the two images at the pixel point (x, y), and m and n are the pixel size of the image. In this article, "original $RMSE$" is used to describe the $RMSE$ between the BT image sampled by the source pattern and the original BT image. "Enhanced $RMSE$" is used to describe the $RMSE$ between the BT image after resolution enhancement and the original BT image. The reduction of the "enhanced $RMSE$" compared to the "original $RMSE$" is used to evaluate the resolution enhancement effect. A larger reduction indicates a better resolution enhancement effect at the image level.

IV. Experiments and Analysis

A. Effect of Enhanced FOV on Resolution Enhancement

In this section, the effect of enhanced FOVs with different spatial resolutions on improving spatial resolution is analyzed. For the experiment, the spatial resolution of the source FOV is set to 30 $\times$ 50 km, which is consistent with the MWRI 18.7 GHz channel. With a step size of 5 km, the spatial resolution of the target pattern in the enhanced FOV (referred to as the enhanced FOV resolution) is specified as 10 km to 25 km and 20 km to 40 km in the cross-track direction and along-track direction, respectively. Note that setting the enhanced FOV resolution to 10 $\times$ 20 km is already beyond the maximum level of resolution that can be improved by applying the BG method, so the higher resolution is not set for the experiments.

To obtain the spatial resolution enhancement effect under different experimental conditions, the simulation scanning results of the source pattern in the reference field and the weighting factors calculated by the BG method under different experimental conditions need to be obtained. The technical route is specified in the following.

In the simulation scanning process, all scanning geometric parameters are set to be consistent with MWRI. In the reference field, the positive direction of the *X*-axis is defined as the along-track direction, whereas the negative direction of the *Y*-axis is defined as the cross-track direction. The line $Y = 1000$ is defined as the forward track of the instrument. The positions of all scanning sampling points in the reference field and the corresponding normalized antenna pattern are then calculated using prior information such as the sampling interval. Finally, the convolution of the antenna pattern of each sampling point and the BT of the corresponding position is calculated to obtain the scanning BT image, as shown in Fig. 4(a). Note that the scan width of MWRI is 1400 km, whereas the width of the reference field is 2000 km. Therefore, the simulation scanning process does not involve the problem of edge processing. In

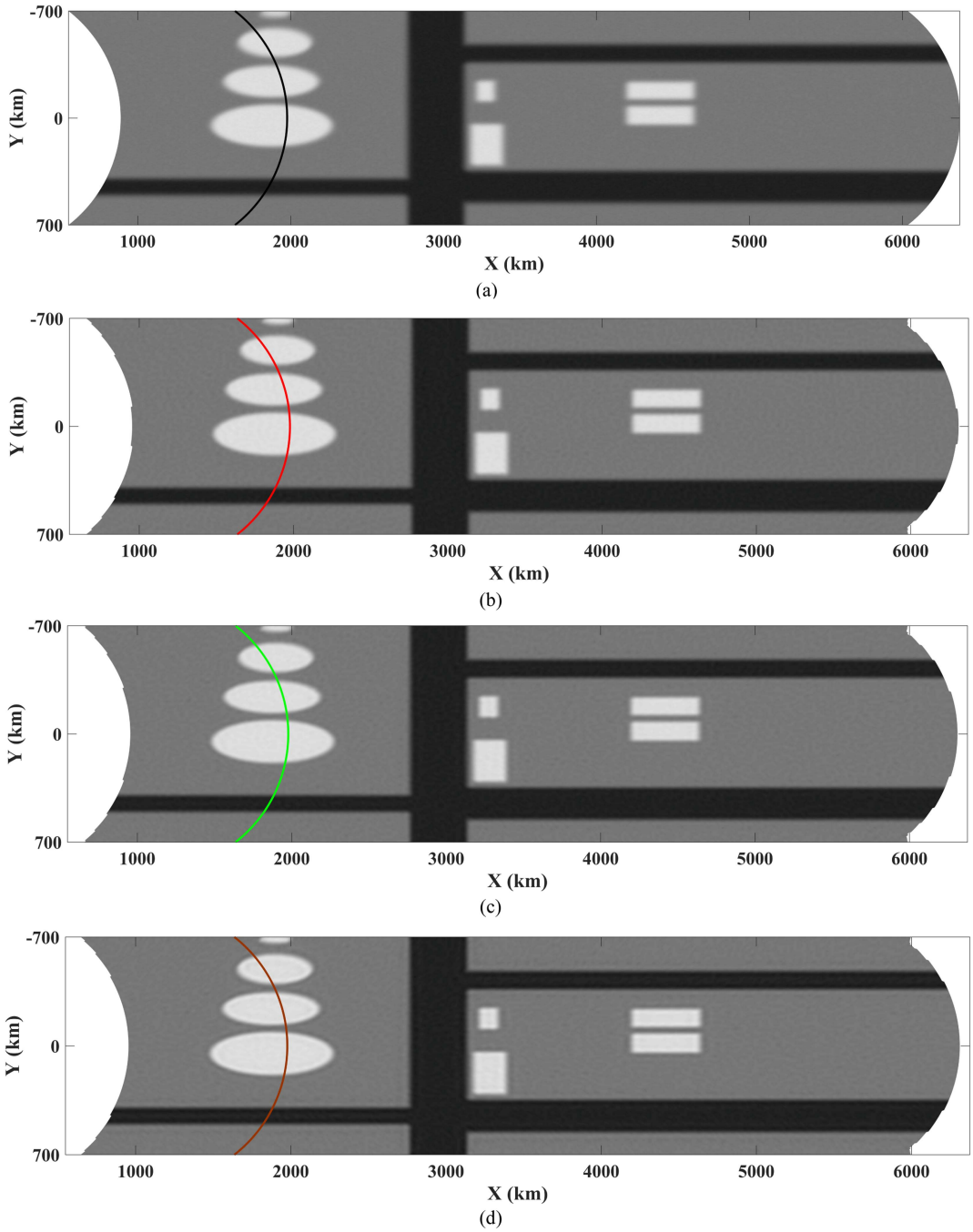

Fig. 4. Simulation scanning results of the source pattern in the reference field and the spatial resolution enhanced images obtained by the BG method at different enhanced FOV resolutions. (a) Scanning result of the source pattern. (b)–(d) Resolution enhancement results when the enhanced FOV resolution is 25 × 35 km, 20 × 30 km, and 10 × 20 km, respectively.

the process of applying the BG method, the weighting factors under different experimental conditions can be obtained by replacing the target pattern during the application process. Then, the resolution enhancement results can be obtained from (2). Examples of resolution enhancement results when the enhanced FOV resolution is 25 × 35 km, 20 × 30 km, and 10 × 20 km are shown in Fig. 4(b)–(d).

Fig. 5(a)–(d) shows the $RMSE$ reduction of the BT image before and after resolution enhancement, the FE, the average BT error, and the overall spatial resolution improvement percentage under the set enhanced FOV resolutions. As shown in Fig. 5(a) and (b), with a decrease in spatial resolution in both directions, although the $RMSE$ reduction becomes larger, the FE also gradually increases. The influence of FE on resolution enhancement can be visually evaluated according to Fig. 4. When the enhanced FOV resolution is set at 10 × 20 km [see Fig. 4(d)], the BT boundary is obvious, and the resolution enhancement effect is the best at the image level. However, large

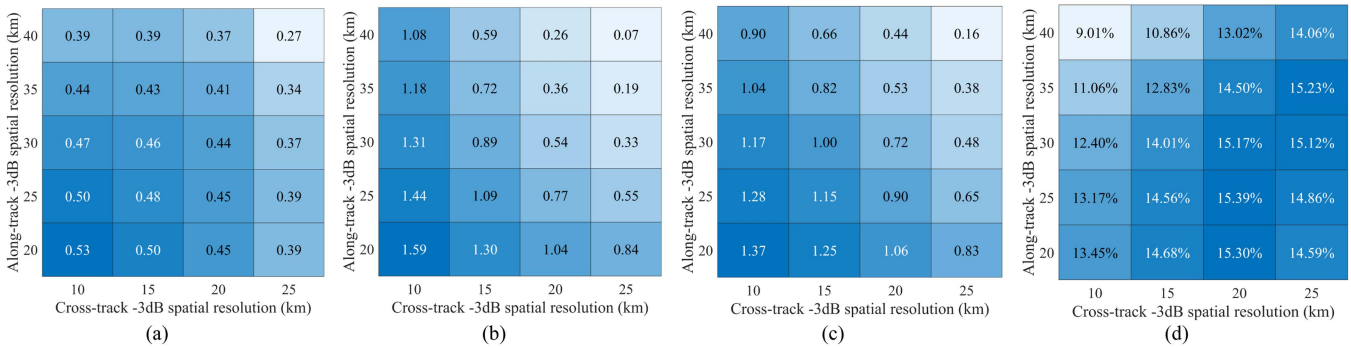

Fig. 5. Parameter changes of the simulation scan results after spatial resolution enhancement at different enhanced FOV resolutions. (a) $RMSE$ reduction (K), (b) FE, (c) average BT error (K), and (d) overall spatial resolution improvement percentage.

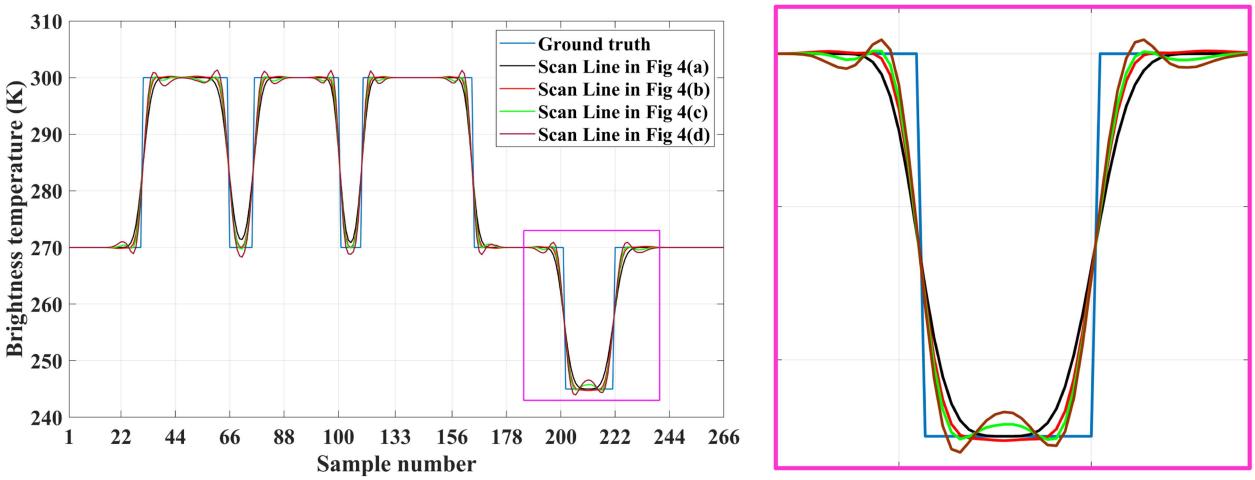

Fig. 6. BT change at the marked scan line of the BT image in Fig. 4 and the real BT change of the reference field. The blue line is the true BT of the reference field, and the black, red, green, and brown lines are the BT at the marked scanning lines in Fig. 4(a)–(d), respectively.

FE leads to abnormal BT changes around the BT boundary [23]. To clearly show this phenomenon, Fig. 6 shows the BT changes of all the BT images in Fig. 4 at the marked scan lines (the influence of noise is removed), where the blue line is the reference field BT, and the black, red, green, and brown lines are the BT at the marked scanning lines in Fig. 4(a)–(d), respectively. As shown in Fig. 6, when the scan line crosses the BT boundary, compared with the black scan line, the BT variations of the other scan lines are closer to the reference field BT. Among them, the higher the enhanced FOV resolution, the closer the BT change of the corresponding scan line is to the reference field, and the greater the resolution improvement at the image level. However, compared with the reference field BT, the green and brown scan lines exhibit abnormal BT increase or decrease when they start to approach or leave the BT boundary. This phenomenon seriously affects the realism of resolution enhanced data. Fig. 5(c) shows the average BT error caused by this phenomenon under different enhanced FOVs. The variation rule is consistent with the FE. In summary, although setting a higher enhanced FOV resolution can make the enhanced BT image obtain a smaller $RMSE$ at the image level, the BT error caused by spatial resolution enhancement should also be considered for remote sensing applications. The BT error can be effectively reduced by selecting an appropriate enhanced FOV resolution.

Furthermore, to verify that the results of the simulation experiment are also valid on the actual data, the visualization experiment is conducted on the actual BT data of MWRI with the same criteria as the simulation experiment. Specifically, the 18.7-GHz horizontally polarized MWRI BT data at 1209 UTC January 15, 2019 in the western Mediterranean region is selected. Fig. 7 shows the original BT distribution of the selected data [see Fig. 7(a)] and the spatial resolution enhanced images obtained when the enhanced FOV resolution is 25 × 35 km [see Fig. 7(b)] and 10 × 20 km [see Fig. 7(c)], respectively. As the figure shows, both resolution enhanced images achieve better results compared to the original BT distribution. Specifically, the strait in the blue enlarged region becomes easier to distinguish, and the bay in the purple enlarged region becomes more obvious. However, compared with Fig. 7(b), the BT in the area near the coastline in Fig. 7(c) shows an abnormal increase or decrease. This result is consistent with the simulation experiment, which

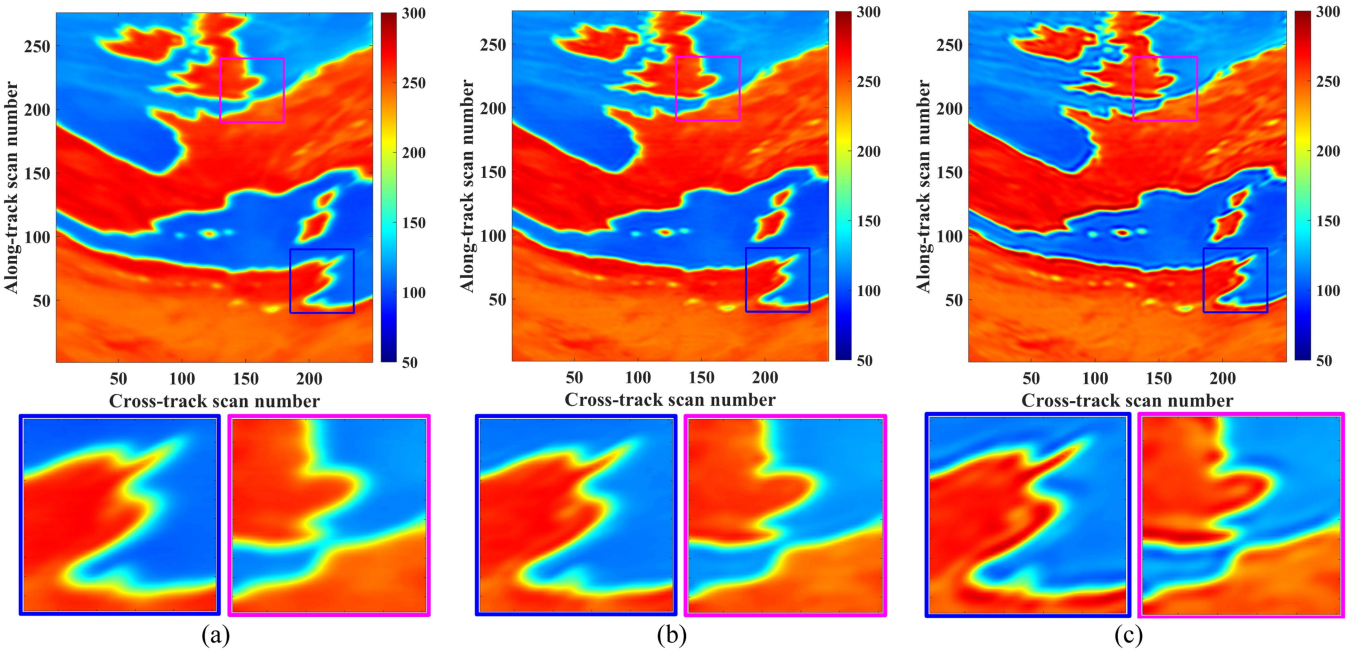

Fig. 7. Spatial resolution enhancement effect obtained by applying different enhanced FOV in actual MWRI measurement scenarios. (a) 18.7-GHz horizontally polarized MWRI original BT distributions at 1209 UTC January 15, 2019. (b) and (c) Spatial resolution enhanced images obtained when the enhanced FOV is 25 × 35 km and 10 × 20 km, respectively.

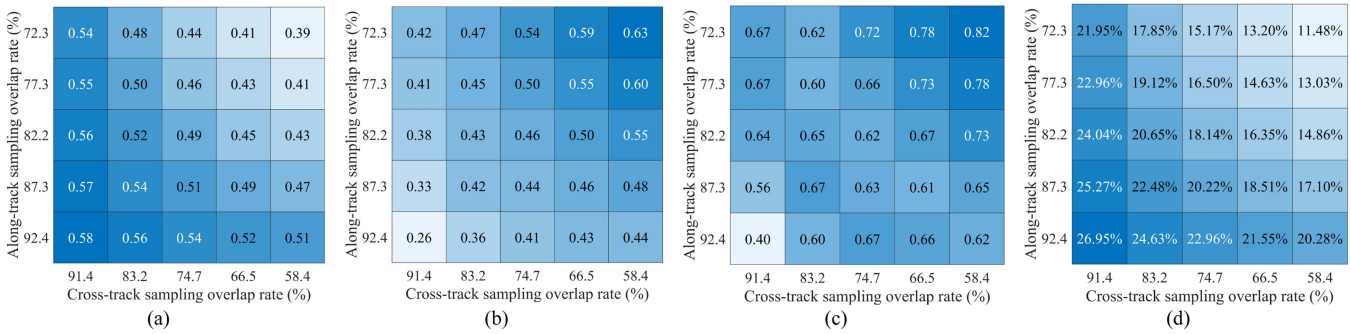

Fig. 8. Parameter changes of the simulation scan results after spatial resolution enhancement at different sampling overlap rates. (a) $RMSE$ reduction (K), (b) FE, (c) average BT error (K), and (d) overall spatial resolution improvement percentage.

TABLE II
ENHANCED SPATIAL RESOLUTION (CROSS-TRACK [KM] × ALONG-TRACK [KM]) OBTAINED BY THE BG METHOD AT DIFFERENT ENHANCED FOV RESOLUTIONS

Along-track \ Cross-track	10 km	15 km	20 km	25 km
20 km	25.6 × 43.7	26.3 × 42.0	27.7 × 40.1	30.0 × 38.4
25 km	24.9 × 44.6	25.6 × 42.8	27.0 × 40.7	29.3 × 38.9
30 km	24.3 × 45.8	24.9 × 43.9	26.1 × 41.7	28.4 × 39.5
35 km	23.6 × 47.6	24.2 × 45.6	25.2 × 43.2	27.3 × 40.5
40 km	23.0 × 49.8	23.5 × 47.8	24.3 × 45.3	26.3 × 42.4

proves the validity of our simulation process and simulation results.

Table II shows the enhanced spatial resolutions achieved by applying the BG method using different enhanced FOV resolutions. It can be observed from the table that when the enhanced FOV resolution in the along-track direction is constant, increasing the enhanced FOV resolution in the cross-track direction leads to higher spatial resolution obtained by the BG method in the cross-track direction. On the other hand, when the enhanced FOV resolution is constant in the cross-track

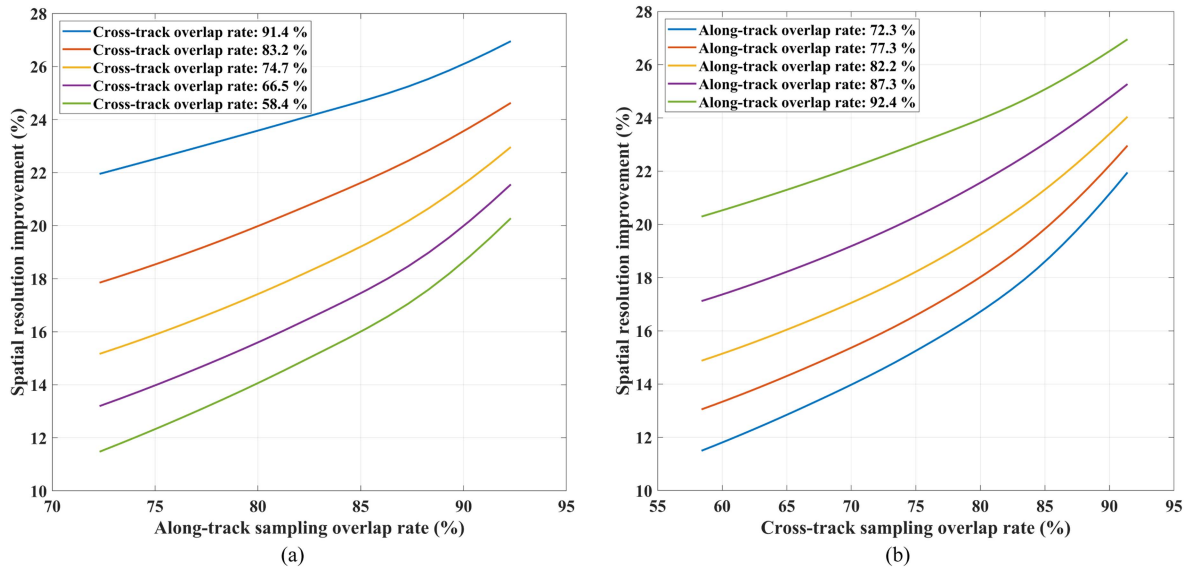

Fig. 9. Changing trend of the spatial resolution improvement percentage with the change of the sampling overlap rate in the (a) along-track or (b) cross-track direction. Different colored lines represent different sample overlap rates in another direction.

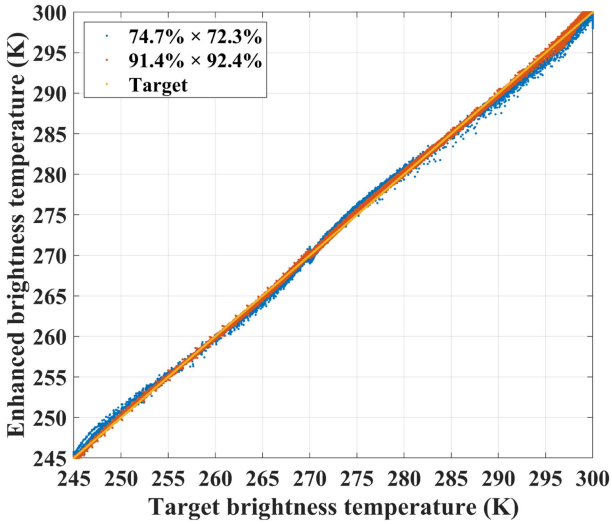

Fig. 10. Correlation between the enhanced BT images and the target BT image under different experimental conditions. The x-coordinate values of the blue and red points represent the BT values of the target BT image, whereas the y-coordinate values represent the BT values of the enhanced BT images when the sampling overlap rates are 74.7% × 72.3% and 91.4% × 92.4%, respectively. The x and y coordinates of the yellow points are the BT values of the target BT image.

direction and decreases in the along-track direction, the number of source patterns involved in resolution enhancement increases, resulting in a more accurate description of the target pattern in the cross-track direction. This leads to higher spatial resolution obtained by applying the BG method in the cross-track direction. Similarly, the spatial resolution in another direction also exhibits the same trend.

Based on the results shown in Fig. 5 and Table II, the MWRI 18.7 GHz channel exhibits relatively better resolution enhancement when the enhanced FOV resolution is set at 25 × 35 km. In this case, the average BT error caused by the FE is 0.38 K, and the spatial resolution can be improved from 30 × 50 km to 27.3 × 40.5 km, resulting in a 15.23% increase in overall spatial resolution.

Table III shows the best enhanced FOV, average BT error, spatial resolution after enhancement, and overall spatial resolution improvement percentage for the other channels in MWRI, which are calculated using the same method. As all channels of MWRI use the same sampling interval, the low-frequency channels with lower spatial resolution have a larger sampling overlapping area, which helps to extract spatial resolution information. Consequently, as the channel center frequency increases, the resolution enhancement effect decreases. Notably, the 89 GHz channel with the highest spatial resolution contains less sampling overlapping information, which makes spatial resolution enhancement unfeasible.

In conclusion, the experimental results presented in this section indicate that selecting an appropriate enhanced FOV is an important factor to improve the spatial resolution of the spaceborne microwave radiometer measurements. By doing so, a better resolution enhancement effect can be achieved, and the BT error caused by spatial resolution enhancement can be effectively reduced.

B. *Effect of Sampling Strategy on Resolution Enhancement*

The sampling overlap rate is the ratio between the overlapping area of adjacent scan FOVs and the area of the complete FOV. A higher sampling overlap rate can be achieved with smaller sampling intervals. In this section, the effect of sampling overlap rate on spatial resolution enhancement is analyzed. In the experiment, the resolution of the source FOV is set to 30 ×50 km, and the resolution of the enhanced FOV is set to 20 ×30 km. Other scanning parameters are consistent with MWRI. With a step size of 2 km, the sampling interval ranges are specified as

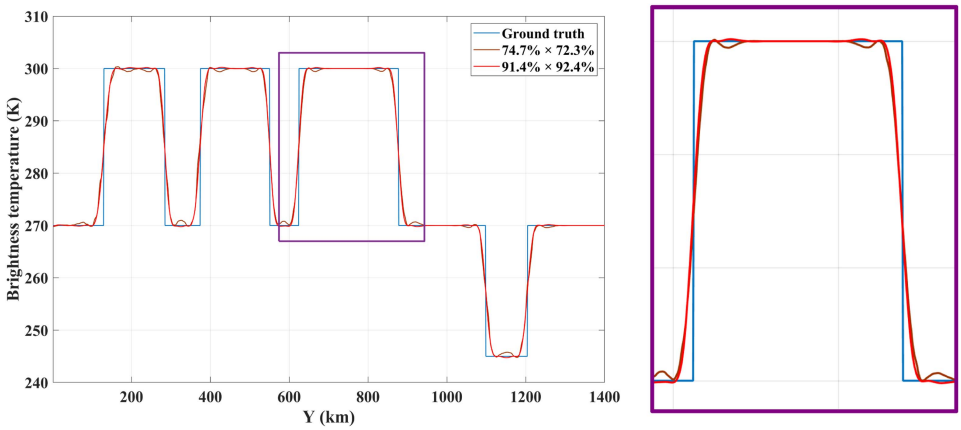

Fig. 11. Change of the true BT and the enhanced BT obtained under different sampling overlapping rates. The blue line is the true BT change of the reference field, whereas the brown and red lines are the BT changes of the enhanced image when the sampling overlap rate is 74.7% × 72.3% and 91.4% × 92.4%, respectively.

TABLE III
BEST ENHANCED FOV CORRESPONDING TO DIFFERENT CHANNELS OF MWRI, AND THE SPATIAL RESOLUTION ENHANCEMENT INFORMATION AND AVERAGE BT ERROR OBTAINED UNDER THE BEST ENHANCED FOV

Channel (GHz)		10.65	18.7	23.8	36.5
Spatial Resolution Info	Original (km)	51 × 85	30 × 50	27 × 45	18 × 30
	Enhanced (km)	43.6 × 63.9	27.3 × 40.5	24.1 × 38.0	16.9 × 27.5
	Improvement Percentage	20.93%	15.23%	13.81%	7.42%
Enhanced FOV (km)		40 × 55	25 × 35	21 × 32	15 × 24
Average BT Error (K)		0.44	0.38	0.42	0.31

TABLE IV
ENHANCED SPATIAL RESOLUTION (CROSS-TRACK [KM] × ALONG-TRACK [KM]) OBTAINED BY THE BG METHOD AT DIFFERENT SAMPLING OVERLAP RATES

Along-track \ Cross-track	91.4%	83.2%	74.7%	66.5%	58.4%
92.4%	22.8 × 35.7	23.4 × 36.9	23.9 × 37.7	24.3 × 38.4	24.7 × 39.1
87.3%	23.2 × 36.5	24.1 × 38.0	24.7 × 39.1	25.2 × 40.0	25.6 × 40.7
82.2%	23.6 × 37.2	24.6 × 38.9	25.3 × 40.2	25.8 × 41.1	26.2 × 41.9
77.3%	23.9 × 37.7	25.0 × 39.7	25.8 × 41.1	26.3 × 42.0	26.8 × 42.8
72.3%	24.2 × 38.2	25.4 × 40.4	26.1 × 41.7	26.7 × 42.7	27.2 × 43.6

2 km to 10 km and 3 km to 11 km in the cross-track direction and along-track direction, respectively. The resulting sampling overlap rates are calculated as 91.4%, 83.2%, 74.7%, 66.5%, and 58.4% in the cross-track direction and 92.4%, 87.3%, 82.2%, 77.3%, and 72.3% in the along-track direction. For MWRI, the sampling overlap rate is 74.7% × 72.3%. Note that achieving a higher sampling overlap rate generally requires setting more sampling points, which leads to reduced integration time and a consequent decrease in the sensitivity of the system. Therefore, higher sampling overlap rates are not set in this section.

The technical route for this experiment is similar to the previous section, and the results are directly given here. Fig. 8(a)–(d) shows the $RMSE$ reduction of the BT image before and after resolution enhancement, the FE, the average BT error, and the overall spatial resolution improvement percentage under different sampling overlap rates. The figures show that as the sampling overlap rate increases, the $RMSE$ reduction becomes larger, the FE and average BT error decrease, and the spatial resolution improvement percentage increases. Table IV presents the enhanced spatial resolutions obtained by applying the BG method at different sampling overlap rates; it can be seen that the higher the sampling overlap rate, the higher the spatial resolution improvement. The changing trend of the spatial resolution improvement percentage with the change of the sampling overlap rate in the along-track and cross-track direction is depicted in Fig. 9(a) and (b), respectively. It can be observed that the sampling overlap rate and the resolution improvement percentage have approximately linear monotonic relationships.

Quantitatively, the best spatial resolution enhancement effect can be achieved when the sampling overlap rate of both directions reaches the maximum. Compared to the sampling strategy of MWRI (74.7% × 72.3%), the average BT error caused by spatial resolution enhancement decreased from 0.72 to 0.4 K, and the spatial resolution improved from 26.1 × 41.7 km to 22.8 × 35.7 km. The spatial resolution improvement percentage increased from 15.17% to 26.95%.

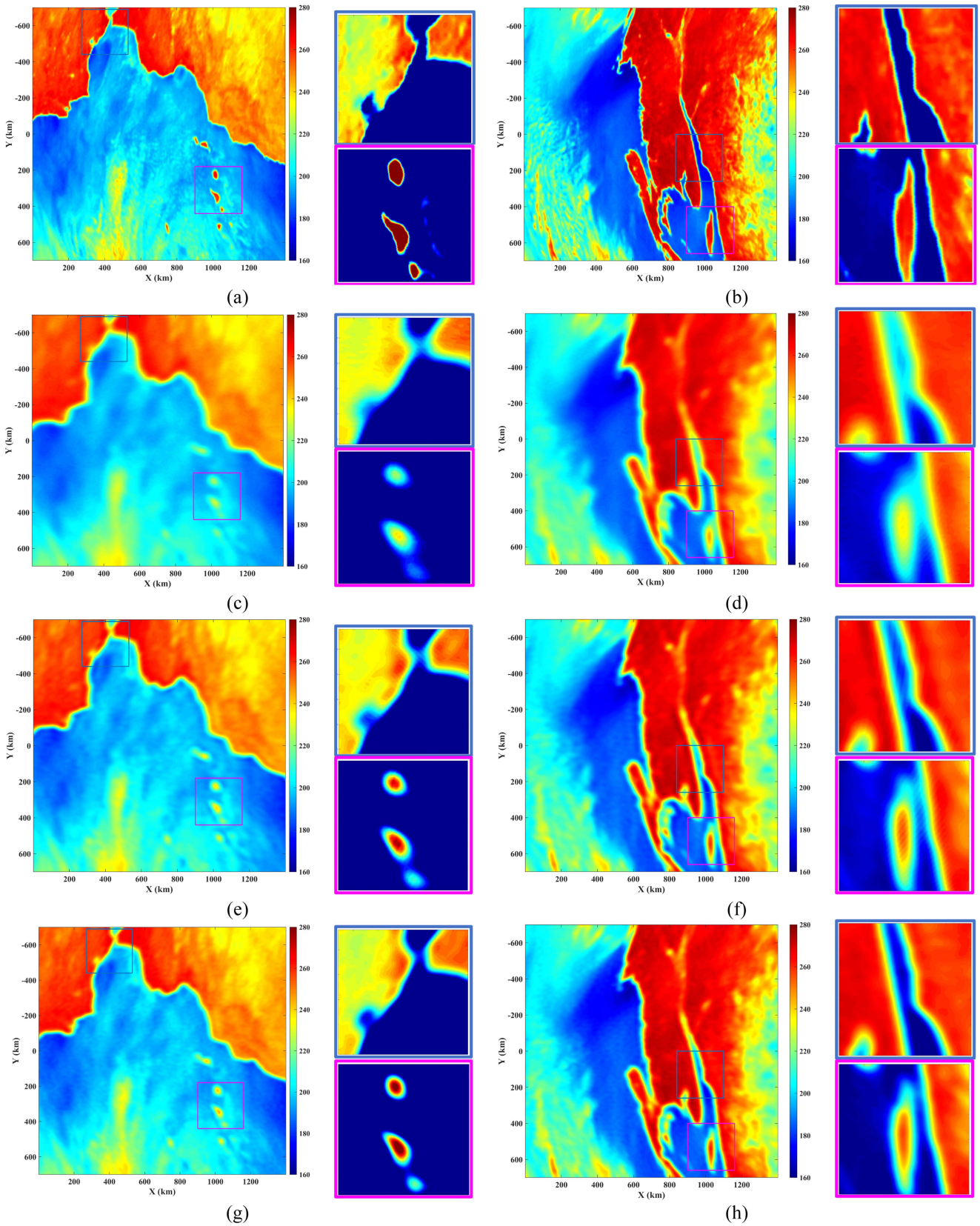

Fig. 12. Spatial resolution enhancement effect obtained by applying different sampling overlap ratios in actual spaceborne radiometer measurement scenarios. (From left to right) Experimental areas in the areas around Morocco (a), (c), (e), (g) and around Quebec, Canada (b), (d), (f), (h). (From top to bottom) 89-GHz horizontally polarized MWRI original BT distributions at 0226 UTC January 11, 2019 (a) and 1646 UTC April 11, 2019 (b). The scanning results of the source pattern (c), (d), and the spatial resolution enhanced images obtained when the sampling overlap ratios are 74.7% $\times$ 72.3% (e), (f) and 91.4% $\times$ 92.4% (g), (h). Note that the BT display ranges of the enlarged areas are reduced, and the values in the same area are consistent.

To illustrate the overall effect of increasing the sampling overlap rate on spatial resolution enhancement, the scanning result of the target pattern (10 × 20 km) in the reference field is used as the target BT image of all the enhanced BT images. Fig. 10 shows the correlation between the enhanced BT images and the target BT image under different experimental conditions. The x-coordinate values of the blue and red points represent the BT values of the target BT image, whereas the y-coordinate values represent the BT values of the enhanced BT images when the sampling overlap rates are 74.7% × 72.3% and 91.4% × 92.4%, respectively. The straight line composed of yellow points is the target reference line, and its horizontal and vertical coordinate values are the BT values of the target BT image. As the figure shows, the red point is closer to the target reference line than the blue point, indicating that when the sampling overlap rate is 91.4% × 92.4%, the enhanced BT image is closer to the target BT image, and the spatial resolution enhancement effect is better.

To illustrate the effect of spatial resolution enhancement more intuitively, we take the position of the line $X = 2000$ in the reference field as an example. Fig. 11 shows the change of the true BT and the enhanced BT obtained under different sampling overlapping rates. The blue line represents the true BT change of the reference field, whereas the brown and red lines represent the BT changes of the enhanced image when the sampling overlap rates are 74.7% × 72.3% and 91.4% × 92.4%, respectively. Compared with the brown line, the BT change of the red line is closer to the true BT when it crosses the BT boundary. In addition, the red line does not exhibit abnormal BT changes similar to the brown line when it approaches or leaves the BT boundary.

Furthermore, to validate our research in more diverse and challenging scenarios, visualization experiment is performed using radiometer measurements from actual spaceborne satellite. Specifically, the 89-GHz horizontally polarized MWRI BT distributions at 0226 UTC January 11, 2019 in the region near Morocco and 1646 UTC April 11, 2019 in the region near southern Quebec, Canada are selected. Fig. 12 shows the original BT distributions of the selected data in different regions [see Fig. 12(a) and (b)], the scanning results of the source pattern [see Fig. 12(c) and (d)], and the spatial resolution enhanced images obtained when the sampling overlap ratios are 74.7% × 72.3% [see Fig. 12(e) and (f)] and 91.4% × 92.4% [see Fig. 12(g) and (h)], respectively. Note that to show the effect more clearly, the BT display ranges of the enlarged areas are reduced, and the values in the same area are consistent. As the figure shows, both resolution enhanced images achieve better results compared to the scanning results. Among them, the higher the sampling overlap rate, the clearer the BT distribution of the enhanced image. Specifically, areas such as straits and islands in the enhanced image with a high sampling overlap rate are easier to distinguish and closer to the original BT. In addition, the enhanced image with high sampling overlap also eliminates the abnormal BT variation near the coastline [see the blue enlarged region in Fig. 12(f) and (h)].

To summarize, increasing the sampling overlap rate of the radiometer can obtain a better resolution enhancement effect and effectively reduce the BT error caused by resolution enhancement. However, achieving a higher sampling overlap rate typically requires setting more sampling points, which reduces the integration time of the radiometer and results in a decrease in the sensitivity of the system. In addition, increasing the number of sampling points also leads to greater computing resource consumption during the spatial resolution enhancement process. Therefore, the sampling strategy should be determined based on the compromise between actual conditions and application requirements.

V. Conclusion

Low spatial resolution is a significant factor restricting the application of spaceborne microwave radiometer data. In this article, the effect of enhanced FOV and sampling strategy on improving the spatial resolution of the radiometer measurements is analyzed using the BG method.

In the experiment of analyzing the effect of enhanced FOV on spatial resolution enhancement, the results show that the higher the enhanced FOV resolution, the greater the BT error caused by resolution enhancement. In addition, when the enhanced FOV resolution in the along-track (cross-track) direction remains unchanged, the enhanced spatial resolution in the cross-track direction is consistent (opposite) with the change of enhanced FOV resolution in the cross-track (along-track) direction. Similarly, the enhanced spatial resolution in the along-track direction also has the same characteristics. Quantitatively, under the MWRI sampling setting, the best spatial resolution enhancement is achieved when the source FOV resolution is 30 × 50 km and the enhanced FOV resolution is set to 25 × 35 km. The enhanced spatial resolution is 27.3 × 40.5 km, and the average BT error is 0.38 K. In the experiment of analyzing the effect of sampling strategy on spatial resolution enhancement, the results show that increasing the sampling overlap rate can reduce the BT error caused by resolution enhancement and obtain a better spatial resolution enhancement effect. Specifically, the best result can be achieved when the sampling overlap rate is set to 91.4% × 92.4%. Compared with the original sampling overlap rate of MWRI, the enhanced spatial resolution can be improved from 26.1 × 41.7 km to 22.8 × 35.7 km, and the average BT error can be reduced from 0.72 to 0.4 K.

In conclusion, choosing an appropriate enhanced FOV can obtain a better resolution enhancement effect and reduce the BT error caused by resolution enhancement. Moreover, increasing the sampling overlap rate can improve the upper limit of resolution enhancement and further reduce the BT error. In the future system design of the radiometer and the application of the BG method, the spatial resolution of the radiometer measurements can be better improved by choosing an appropriate sampling strategy and enhanced FOV under the premise of balancing the sampling overlap rate and system sensitivity.

VI. Discussion

The observation data of the microwave radiometer can be used to retrieve various geophysical parameters, providing important support for research in meteorology, hydrology, agriculture, and

other fields. In the design of future radiometer systems, better spatial resolution can be achieved indirectly by adjusting the observation of the radiometer itself, and then more accurate data products can be generated.

An advantage of applying the conclusions of this article to future radiometer designs is given here. In the design of future radiometers, higher spatial resolution can be achieved by increasing the antenna aperture. However, this approach may lead to higher antenna installation costs and potentially hinder the radiometer's ability to achieve full-coverage observations within the same scan configuration. Consequently, an indirect way to improve spatial resolution may be a better choice. Specifically, researchers can maintain full-coverage observations by selecting smaller antenna apertures, and indirectly achieve higher spatial resolution by adjusting the sampling overlap rate.

Based on this article, the following issue still needs further research. When using radiometer data for multichannel collaborative inversion, resampling must be considered to make the data of different detection channels have a consistent spatial resolution. Downgrading high resolution to low resolution is easy, but it results in the loss of small-scale information. Therefore, enhancing low spatial resolution to match high spatial resolution is a better approach. However, in general, the observation information carried by the radiometer itself is not enough to enhance the spatial resolution of the low-frequency channel to match the high-frequency channel. The experimental results in this article are obtained under the premise that the BG method does not amplify the noise. This means that a better spatial resolution can be obtained by appropriately relaxing the restriction on noise. Therefore, under the premise of choosing an appropriate sampling overlap rate and noise amplification strategy, it is possible to match the spatial resolution between channels by improving the spatial resolution. The specific parameter settings should be determined by the sensitivity of the parameters to be inverted to noise. This will be one of the focuses of our future research.

REFERENCES

[1] S. Sabaghy, J. P. Walker, L. J. Renzullo, and T. J. Jackson, "Spatially enhanced passive microwave derived soil moisture: Capabilities and opportunities," *Remote Sens. Environ.*, vol. 209, pp. 551–580, May 2018.

[2] M. Piles, D. Entekhabi, and A. Camps, "A change detection algorithm for retrieving high-resolution soil moisture from SMAP radar and radiometer observations," *IEEE Trans. Geosci. Remote Sens.*, vol. 47, no. 12, pp. 4125–4131, Dec. 2009.

[3] M. Choi and Y. Hur, "A microwave-optical/infrared disaggregation for improving spatial representation of soil moisture using AMSR-E and MODIS products," *Remote Sens. Environ.*, vol. 124, pp. 259–269, Sep. 2012.

[4] M. Alparone, F. Nunziata, C. Estatico, and M. Migliaccio, "A multichannel data fusion method to enhance the spatial resolution of microwave radiometer measurements," *IEEE Trans. Geosci. Remote Sens.*, vol. 50, no. 3, pp. 2213–2221, Mar. 2021.

[5] E. Santi, "An application of the SFIM technique to enhance the spatial resolution of spaceborne microwave radiometers," *Int. J. Remote Sens.*, vol. 31, no. 9, pp. 2419–2428, May 2010.

[6] W. Hu, W. Zhang, S. Chen, L. Xin, and L. Leo, "A deconvolution technology of microwave radiometer data using convolutional neural networks," *Remote Sens.*, vol. 10, no. 2, pp. 275–292, Feb. 2018.

[7] W. Hu, Y. Li, W. Zhang, S. Chen, L. Xin, and L. Leo, "Spatial resolution enhancement of satellite microwave radiometer data with deep residual convolutional neural network," *Remote Sens.*, vol. 11, no. 7, pp. 771–790, Mar. 2019.

[8] T. Hu, F. Zhang, W. Li, W. Hu, and R. Tao, "Microwave radiometer data superresolution using image degradation and residual network," *IEEE Trans. Geosci. Remote Sens.*, vol. 57, no. 11, pp. 8954–8967, Nov. 2019.

[9] P. C. Hanson, *Rank-Deficient Discrete Ill-Posed Problems*. Philadelphia, PA, USA: SIAM, 1998.

[10] A. Stogryn, "Estimates of brightness temperatures from scanning radiometer data," *IEEE Trans. Antennas Propag.*, vol. AP-26, no. 5, pp. 720–726, Sep. 1978.

[11] M. R. Farrar and E. A. Smith, "Spatial resolution enhancement of terrestrial features using deconvolved SSM/I microwave brightness temperatures," *IEEE Trans. Geosci. Remote Sens.*, vol. 30, no. 2, pp. 349–355, Mar. 1992.

[12] W. D. Robinson, C. Kummerow, and W. S. Olson, "A technique for enhancing and matching the resolution of microwave measurements from the SSM/I instrument," *IEEE Trans. Geosci. Remote Sens.*, vol. 30, no. 3, pp. 419–429, May 1992.

[13] R. Sethmann, G. Heygster, and B. Burns, "Image deconvolution techniques for reconstruction of SSM/I data," in *Proc. Int. Geosci. Remote Sens. Symp.*, Jun. 1991, pp. 2377–2380.

[14] R. Sethmann, B. A. Burns, and G. C. Heygster, "Spatial resolution improvement of SSM/I data with image restoration techniques," *IEEE Trans. Geosci. Remote Sens.*, vol. 32, no. 6, pp. 1144–1151, Nov. 1994.

[15] D. G. Long, "Scatterometer backscatter imaging using Backus–Gilbert inversion," *IEEE Trans. Geosci. Remote Sens.*, vol. 57, no. 6, pp. 3179–3190, Jun. 2019.

[16] F. Lenti, F. Nunziata, C. Estatico, and M. Migliaccio, "On the spatial resolution enhancement of microwave radiometer data in Banach spaces," *IEEE Trans. Geosci. Remote Sens.*, vol. 52, no. 3, pp. 1834–1842, Mar. 2014.

[17] F. Lenti, F. Nunziata, C. Estatico, and M. Migliaccio, "Spatial resolution enhancement of earth observation products using an acceleration technique for iterative methods," *IEEE Geosci. Remote Sens. Lett.*, vol. 12, no. 2, pp. 269–273, Feb. 2015.

[18] F. Lenti, F. Nunziata, C. Estatico, and M. Migliaccio, "Conjugate gradient method in Hilbert and Banach spaces to enhance the spatial resolution of radiometer data," *IEEE Trans. Geosci. Remote Sens.*, vol. 54, no. 1, pp. 397–406, Jan. 2016.

[19] D. G. Long and M. J. Brodzik, "Optimum image formation for spaceborne microwave radiometer products," *IEEE Trans. Geosci. Remote Sens.*, vol. 54, no. 5, pp. 2763–2779, May 2016.

[20] D. G. Long and D. L. Daum, "Spatial resolution enhancement of SSM/I data," *IEEE Trans. Geosci. Remote Sens.*, vol. 36, no. 2, pp. 407–417, Mar. 1998.

[21] D. G. Long, M. J. Brodzik, and M. A. Hardman, "Enhanced-resolution SMAP brightness temperature image products," *IEEE Trans. Geosci. Remote Sens.*, vol. 57, no. 7, pp. 4151–4163, Jul. 2019.

[22] T. Maeda, Y. Taniguchi, and K. Imaoka, "GCOM-W1 AMSR2 level 1R product: Dataset of brightness temperature modified using the antenna pattern matching technique," *IEEE Trans. Geosci. Remote Sens.*, vol. 54, no. 2, pp. 770–782, Feb. 2016.

[23] T. Maeda, "Spatial resolution enhancement algorithm based on the Backus–Gilbert method and its application to GCOM-W AMSR2 data," *IEEE Trans. Geosci. Remote Sens.*, vol. 58, no. 4, pp. 2809–2816, Apr. 2020.

[24] H. Yang, J. Shang, L. Lu, J. He, and H. Xu, "Study of channel resolution matching of spaceborne microwave radiometer and its application in MWRI of FY-3 satellite," *Aerosp. Shanghai*, vol. 29, no. 1, pp. 23–28, Jan. 2012.

[25] H. Yang et al., "The FengYun-3 microwave radiation imager on-orbit verification," *IEEE Trans. Geosci. Remote Sens.*, vol. 49, no. 11, pp. 4552–4560, Nov. 2011.

Zhou Zhang is currently working toward the Ph.D. degree in electromagnetic field and microwave technology with the National Space Science Center, Chinese Academy of Sciences, Beijing, China.

His research interests include geolocation correction and spatial resolution enhancement of microwave radiometer data.

Zhenzhan Wang received the Ph.D. degree in space physics from the Graduate University of Chinese Academy of Sciences (CAS), Beijing, China, in 2005.

He was one of the selected candidates of "Hundred Talents Program" of CAS in 2008. He is currently a CAS "Hundred Talents Program" Professor with the National Space Science Center, and the Deputy Director of the CAS Key Laboratory of Microwave Remote Sensing. His research interests include microwave radiation measurement technology, the retrieval algorithm and applied research of atmospheric and oceanic parameters, the calibration technology and methods of the microwave polarimetric radiometers, as well as mechanism and applications of atmosphere detection at terahertz.

Wenming He is currently working toward the Ph.D. degree in electromagnetic field and microwave technology with the National Space Science Center, Chinese Academy of Sciences, Beijing, China.

Her research interests include the application of ground-based and spaceborne microwave spectrometers for atmospheric parameter profiles retrieval.

Xiaolin Tong received the Ph.D. degree in electromagnetic field and microwave technology from Huazhong University of Science and Technology, Wuhan, China, in 2015.

He was a Postdoctoral Scholar with the National Space Science Center, Chinese Academy of Sciences, Beijing, China, where he is currently an Associate Professor. His research interests include remote sensing of sea surface, microwave remote sensing, with multifrequency microwave radiometer.